Validation of Collection 6 MODIS land surface temperature products using in situ measurements

Si-Bo Duan [a], Zhao-Liang Li [a,b,*], Hua Li [c], Frank-M., Göttsche [d], Hua Wu [b], Pei Leng [a], César Coll [e], and Zhengming Wan [f]

[a] Key Laboratory of Agri-informatics, Ministry of Agriculture/Institute of Agricultural Resources and Regional Planning, Chinese Academy of Agricultural Sciences, Beijing 100081, China

[b] State Key Laboratory of Resources and Environment Information System, Institute of Geographic Sciences and Natural Resources Research, Chinese Academy of Sciences, Beijing, 100101, China

[c] State Key Laboratory of Remote Sensing Science, Institute of Remote Sensing and Digital Earth, Chinese Academy of Sciences, Beijing 100101, China

[d] Karlsruhe Institute of Technology (KIT), Hermann-von-Helmholtz-Platz 1, 76344 Eggenstein-Leopoldshafen, Germany

[e] Department of Earth Physics and Thermodynamics, Faculty of Physics, University of Valencia, 46100 Burjassot, Spain

[f] Earth Research Institute, University of California, Santa Barbara, CA 93106, USA

Author to whom correspondence should be addressed; E-Mail: lizhaoliang@caas.cn

Abstract： Land surface temperature (LST) is an important parameter at the land-atmosphere interface. The Collection 6 (C6) MODIS LST products are publicly available. Three refinements were performed over bare soil surfaces in the C6 MODIS LST products when compared with the Collection 5 (C5) MODIS LST products. To facilitate the use of the LST products in a wide range of applications, it is necessary to comprehensively evaluate the accuracies of the C6 MODIS LST products. In this study, we validated the C6 MODIS LST products using the temperature-based method

over various land cover types, including grassland, cropland, cropland/natural vegetation mosaic, Gobi, sandy dune, and desert steppe. In situ measurements were collected from sites under different atmospheric and surface conditions, including six SURFRAD sites in the United States, two KIT sites in Portugal and Namibia, and four HiWATER sites in China. In general, the accuracies of the C6 MODIS LST products at night are better than those during daytime. The daytime RMSE varies from approximately 1.5 K to 5.6 K, whereas the night-time RMSE is less than 2 K at all sites except for the HiWATER SSW site. Furthermore, the accuracies of the C6 MODIS LST products were compared with those of the C5 MODIS LST products over bare soil surfaces. The C6 MODIS LST products are in excellent agreement with the in situ LST measurements at the KIT Gobabeb site, with biases of 0.36 K during the day and 0.24 K at night, and RMSEs of 1.5 K during daytime and 0.74 K during night-time. However, there are no improvements in the accuracies of the C6 MODIS LST products when compared with the C5 MODIS LST products due to further overestimation of emissivities at the four HiWATER sites.

Key words: Land surface temperature, MODIS, temperature-based validation method, split-window algorithm, in situ measurements.

1. Introduction

Land surface temperature (LST) is an important climate variable, which is related to surface energy and water balance. It is also a key parameter for various studies including hydrology, climatology, environment, and ecology (Anderson et al., 2008; Duan et al., 2014; Sandholt et al., 2002; Weng, 2009). For instance, satellite-derived LST has been used in land cover and land-cover change analysis (Lambin and Ehrlich, 1997), in estimation and parameterization of surface fluxes (Lu et al., 2013), and in drought monitoring and surface soil moisture estimation (Wan et al., 2004; Leng et al., 2014). LST has been identified as an important Earth Surface Data Record (ESDR) by NASA. Furthermore, LST has been accepted and defined as an Environmental Climate Variable (ECV) by the Global Climate Observing System (GCOS).

The Moderate Resolution Imaging Spectroradiometer (MODIS) sensor is one of the key instruments on the Terra and Aqua platforms of the NASA Earth Observing System. MODIS can provide observational overlap and continuity in conjunction with the Advanced Very High Resolution Radiometer (AVHRR) onboard the NOAA's operational polar-orbiting satellites and the Visible Infrared Imaging Radiometer Suite (VIIRS) onboard the Suomi National Polar-Orbiting Partnership (S-NPP) satellite. Two LST retrieval algorithms were developed to generate the MODIS LST products. One algorithm is the generalized split-window (GSW) algorithm (Becker and Li, 1990; Wan and Dozier, 1996), which generates LST products at 1 km resolution. The other algorithm is the physics-based day/night algorithm (Wan and Li, 1997), which generates LST products at approximately 5 km (Collection 4, C4) and 6 km (Collection 5, C5) resolution.

The C4 and C5 MODIS LST products were validated using the temperature-based (T-based) and radiance-based (R-based) methods over various sites, including bare soil, grassland, silt playa, cropland, and in-land water (Wan et al., 2002, 2004; Wan and Li, 2008; Wan, 2008, 2014; Coll et al., 2005, 2009). The results indicate that the accuracies of the MODIS LST products are better than 1 K over most sites except for bare soil sites. Three refinements were performed in the Collection 6 (C6) MODIS GSW LST algorithm over bare soil surfaces to improve the accuracies of the MODIS LST products (Wan, 2014). The C6 MODIS LST products are publicly available for the user community. Assessing the accuracies of the C6 MODIS LST products will help to facilitate the use of the LST products in a wide range of applications.

The main objective of this study is to comprehensively validate the C6 MODIS LST products using in situ measurements over various land cover types, including grassland, cropland, cropland/natural vegetation mosaic, Gobi, sandy dune, and desert steppe. This paper is organized as follows: Sections 2 and 3 introduces the MODIS LST products and in situ measurements, respectively, Section 4 describes the methodologies used in this study, Section 5 and 6 presents the results and discussion of the validation of the C6 MODIS LST products, and the last section provides the

conclusions of the study.

2. MODIS LST products

The MODIS level-2 LST products (MOD11_L2 and MYD11_L2) were retrieved with the GSW LST algorithm from brightness temperatures in MODIS bands 31 and 32 (Becker and Li, 1990; Wan and Dozier, 1996). The GSW LST algorithm is written as:

$$T_s = b_0 + \left(b_1 + b_2\frac{1-\varepsilon}{\varepsilon} + b_3\frac{\Delta\varepsilon}{\varepsilon^2}\right)\frac{T_{31}+T_{32}}{2} + \left(b_4 + b_5\frac{1-\varepsilon}{\varepsilon} + b_6\frac{\Delta\varepsilon}{\varepsilon^2}\right)\frac{T_{31}-T_{32}}{2} \quad (1)$$

where T_s is the LST, ε and $\Delta\varepsilon$ are the mean and difference of the emissivities in bands 31 and 32. The regression coefficients b_k (k=0-6) depend on viewing zenith angle (VZA), surface air temperature (T_a), and atmospheric column water vapor (CWV). These coefficients were derived from regression analysis of radiative transfer simulation data for LST values varying from T_a-16 K to T_a+16 K.

To improve the accuracies of the MODIS LST products, three refinements were performed in the C6 MODIS GSW LST algorithm over bare soil surfaces (Wan, 2014). First, two separate sets of coefficients were used to retrieve daytime and night-time LST over bare soil surfaces in the hot and warm bare soil zone within latitude range from −38° to 49.5°. In the original GSW LST algorithm, one set of coefficients was used to retrieve daytime and night-time LST for each group of similar land cover types. Second, the emissivity differences in MODIS bands 31 and 32 over bare soil surfaces were adjusted. Third, a quadratic term of the difference between brightness temperatures in bands 31 and 32 was added into the original GSW LST algorithm. The refined GSW LST algorithm is expressed as:

$$\begin{aligned} T_s = {} & b_0 + \left(b_1 + b_2\frac{1-\varepsilon}{\varepsilon} + b_3\frac{\Delta\varepsilon}{\varepsilon^2}\right)\frac{T_{31}+T_{32}}{2} \\ & + \left(b_4 + b_5\frac{1-\varepsilon}{\varepsilon} + b_6\frac{\Delta\varepsilon}{\varepsilon^2}\right)\frac{T_{31}-T_{32}}{2} + b_7\left(T_{31}-T_{32}\right)^2 \end{aligned} \quad (2)$$

The MODIS LST products were downloaded from the Reverb website (http://reverb.echo.nasa.gov/). The MODIS Reprojection Tool (MRTSwath) was used

to convert the MOD11_L2 and MYD11_L2 products from the sinusoidal projection in HDF format into a geographic projection in GeoTiff format. The science data set layers LST, LSE, and quality control (QC) were extracted from the MOD11_L2 and MYD11_L2 products. Only high-quality LST data (i.e., QC=0) were used in this study.

3. In situ measurements

3.1. SURFRAD sites

The Surface Radiation Budget Network (SURFRAD) was established in 1993 with a primary objective of supporting climate research with accurate, continuous, long-term measurements of the surface radiation budget over the United States (Augustine et al., 2000). Six SURFRAD sites operated in climatologically diverse regions and represented various land cover types were selected in this study. Fig. 1 shows the ground photographs of the six sites. Table 1 summarizes the detailed information on the six sites. These sites provide quality-controlled measurements of surface upwelling and downwelling longwave radiations along with other meteorological parameters every 3 minutes before 2009 or every 1 minute after 2009. The upwelling and downwelling longwave radiations were measured by two pyrgeometers (Eppley Precision Infrared Radiometer, spectral range 3-50 μm) deployed at a 10-meter high tower. The spatial representativeness of the pyrgeometer measurements is approximately 70×70 m^2 (Guillevic et al., 2014). The ground-based measurements from the SURFRAD sites are good reference data sets for long-term LST validation (Li et al., 2014). These measurements have been widely used to evaluate satellite-derived LST products, e.g., ASTER (Wang and Liang, 2009), GOES (Yu et al., 2012; Xu et al., 2014), and VIIRS (Guillevic et al., 2014; Liu et al., 2015).

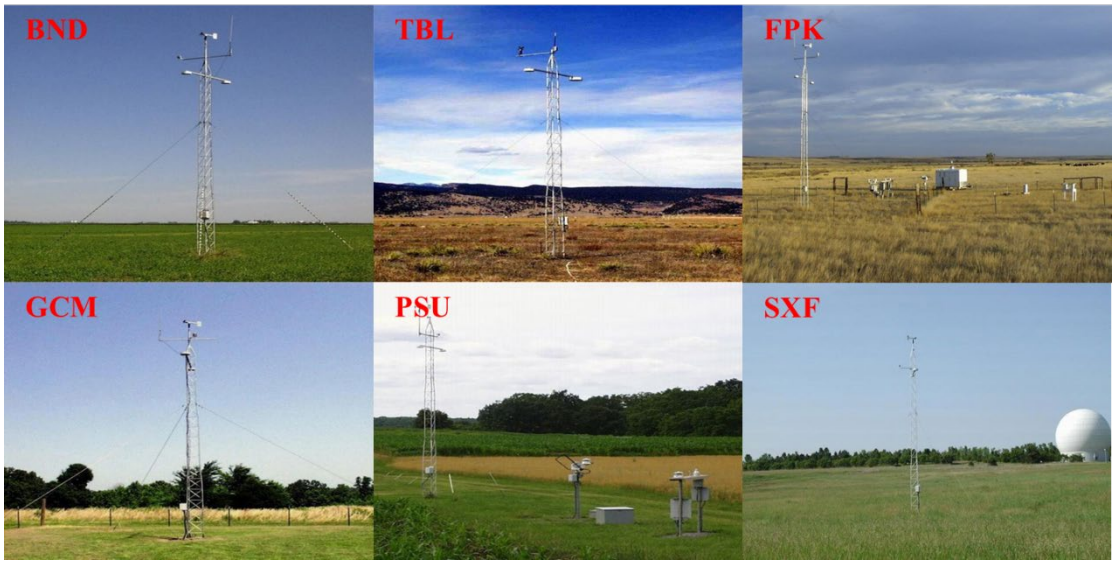

Fig. 1. Ground photographs of the six SURFRAD sites.

Table 1. Detailed information on the six SURFRAD sites.

Site *	Latitude	Longitude	Elevation	Land cover type	Time period (d/m/y)
BND	40.052° N	88.373° W	230 m	Cropland	01/01/2004-31/12/2005
TBL	40.125° N	105.237° W	1689 m	Grassland	01/01/2004-31/12/2005
FPK	48.308° N	105.102° W	634 m	Grassland	01/01/2004-31/12/2005
GCM	34.255° N	89.873° W	98 m	CNVM #	01/01/2004-31/12/2005
PSU	40.720° N	77.931° W	376 m	CNVM #	01/01/2004-31/12/2005
SXF	43.734° N	96.623° W	473 m	Cropland	01/01/2004-31/12/2005

* BND: Bondville, Illinois, TBL: Table Mountain, Boulder, Colorado, FPK: Fort Peck, Montana, GCM: Goodwin Creek, Mississippi, PSU: Penn. State Univ., Pennsylvania, and SXF: Sioux Falls, South Dakota.

CNVM: Cropland/natural vegetation mosaic.

3.2. KIT sites

To enable the continuous validation of the LST products derived from MSG/SEVIRI data over several years, Karlsruhe Institute of Technology (KIT, Germany) operates four permanent LST validation stations, i.e., Evora (Portugal), Dahra (Senegal), Gobabeb (Namibia), and RMZ Farm/Farm Heimat (Namibia). The four stations were set up over large, thermally homogeneous, and flat areas in different climate zones. In this study, the in situ LST measurements over the Evora site in Portugal and the Gobabeb site in Namibia were used to evaluate the C6 MODIS LST products. Fig. 2 shows the ground photographs of the two sites. Table 2

summarizes the detailed information on the two sites.

The Evora LST validation station is located about 12 km south-west of the town of Evora in the Alentejo region, Portugal. The dominant vegetation types at the station are isolated groups of evergreen oak trees and grassland (Kabsch et al., 2008, Trigo et al., 2008). The climate at the station is warm temperate with hot, dry summers, annual temperature averages between 15 °C and 16 °C and an average annual precipitation of 669 mm. The in situ measurements are collected every minute by three KT-15.85 IIP infrared radiometers, observing the sunlit background, a tree crown, and the sky at 53° zenith angle, which is used to estimate atmospheric downwelling radiance. The KT-15.85 IIP measures thermal infrared radiance in the 9.6-11.5 μm domain and obtains brightness temperatures with an absolute accuracy of ±0.3 K. Surface emissivity was estimated using fixed end-member fractions (tree=32%, grass/ground=68%), i.e., the temporal dependence of the cover fractions was ignored (Ermida et al., 2014). The KT-15.85 IIP emissivity was set to a static value of 0.974, which is a typical value for vegetation and close to the corresponding LSA SAF emissivity for SEVIRI channel 9 over Evora.

The Gobabeb LST validation station is located on the large gravel plains (several thousand km^2) of the Namib Desert in Namibia, which are covered by a highly homogeneous mixture of gravel, sand and sparse desiccated grass. Due to the hyper-arid desert climate, the site is spatially and temporally highly stable and, therefore, ideal for long-term validation of satellite products (Göttsche et al., 2013, 2016). The long-term average annual temperature at the Gobabeb site is 21.1 °C whereas the average annual precipitation is less than 100 mm and highly variable. Three KT-15.85 IIP infrared radiometers were deployed at the Gobabeb site. Two radiometers with a field of view (FOV) of 8.5° are mounted next to each other at 25 m height and observe an area of about 14 m^2 each. The other radiometer views the sky at 53° zenith angle. All station measurements are collected once per minute. The surface emissivity of the gravel plain is considered constant and is estimated as 0.94 (Göttsche and Hulley, 2012).

Fig. 2. Ground photographs of the two KIT sites.

Table 2. Detailed information on the two KIT sites.

Site	Latitude	Longitude	Elevation	Land cover type	Time period (d/m/y)
Evora	38.5403° N	8.00328° W	227 m	Savannas	01/01/2010-31/12/2010
Gobabeb	23.5510° S	15.0514° E	421 m	Gravel	01/01/2010-31/12/2010

3.3. HiWATER sites

The Heihe Watershed Allied Telemetry Experimental Research (HiWATER) is a comprehensive eco-hydrological experiment taking place in the Heihe River Basin, the second largest inland river basin in the arid regions of northwest China (37.7°–42.7° N, 97.1°–102.0° E). It designed from an interdisciplinary perspective to address problems that include heterogeneity, scaling, uncertainty, and closing of the water cycle at the watershed scale (Li et al., 2013). We used the ground-based measurements at four sites over three land surface types, i.e., Gobi (GB), sand dune (SSW), and desert steppe (HZZ and JCHM). The four sites are located in large flat areas around the oasis. Fig. 3 shows the ground photographs of the four sites. Table 3 summarizes the detailed information on the four sites.

The GB site consists of small gravel, bare soil, and small Alhagi sparsifolia. The SSW site is more uniformly, but sparsely covered by Alhagi sparsifolia. The sand dune at the SSW site is approximately 10 to 20 m high and the sand is primarily composed of quartz. The HZZ and JCHM sites consist of bare soil and small Alhagi sparsifolia.

The GB and SSW sites are each equipped with one Kipp & Zonen CNR1 net

212 radiometer, which observes the surface at nadir from a 6 m height. The HZZ and
213 JCHM sites are each equipped with two Apogee SI-111 infrared radiometers. One
214 radiometer observes the surface at nadir from a 4 m height with a footprint of 8 m^2 at
215 the JCHM site or a 2.65 m height with a footprint of 3.6 m^2 at the HZZ site. The other
216 radiometer views the sky at an effective angle of approximately 55° from zenith to
217 measure the atmospheric downwelling radiance. The SI-111 infrared radiometers and
218 CNR1 net radiometers are collected once per minute. Surface emissivity at the HZZ
219 and JCHM sites were measured using the ABB BOMEM MR304 spectroradiometers.
220 A constant emissivity value of 0.97 was obtained for the HZZ and JCHM sites. More
221 detailed information on the four sites can be found in Li et al. (2014).
222

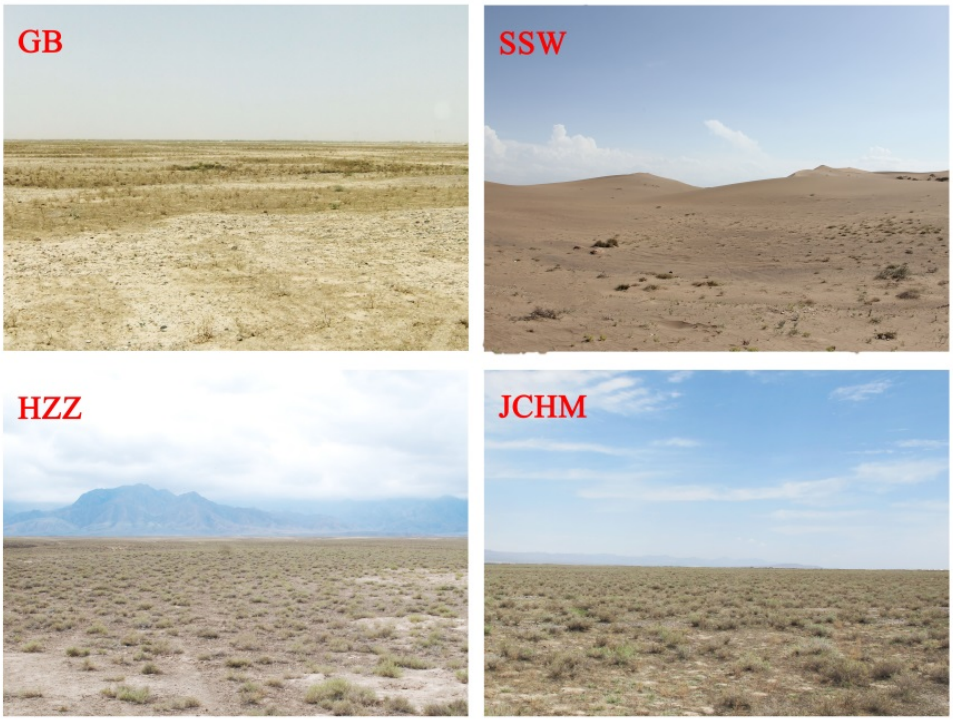

223
224 Fig. 3. Ground photographs of the four HiWATER sites.

225

226 Table 3. Detailed information on the four HiWATER sites.

Site	Latitude	Longitude	Elevation	Land cover type	Time period (d/m/y)
GB	38.9150° N	100.3042° E	1567 m	Gobi	01/07/2012-30/06/2016
SSW	38.7892° N	100.4933° E	1555 m	Sand dune	01/07/2012-30/06/2016
HZZ	38.7652° N	100.3186° E	1735 m	Desert steppe	01/07/2012-30/06/2016
JCHM	38.7781° N	100.6967° E	1625 m	Desert steppe	01/07/2012-30/06/2016

4. Methodologies

4.1. In situ LST estimation

For the pyrgeometers at the SURFRAD sites and the CNR1 net radiometers at the HiWATER sites, the in situ LST measurements were estimated from the upwelling and downwelling longwave radiations using the Stefan-Boltzmann law:

$$T_s = \left[\frac{F^{\uparrow} - (1-\varepsilon_b) F^{\downarrow}}{\sigma \varepsilon_b} \right]^{1/4} \quad (3)$$

where T_s is the LST, $F^{\uparrow}$ is the surface upwelling longwave radiation, $F^{\downarrow}$ is the atmospheric downwelling longwave radiation, σ is the Stefan-Boltzmann constant (5.67×10^{-8} W m^{-2} K^{-4}), ε_b is the surface broadband emissivity, which was estimated from a spectral-to-broadband linear regression equation (Wang et al., 2005):

$$\varepsilon_b = 0.2122\varepsilon_{29} + 0.3859\varepsilon_{31} + 0.4029\varepsilon_{32} \quad (4)$$

where ε_{29}, ε_{31}, and ε_{32} are the surface narrow-band emissivities of MODIS bands 29 (8.3 μm), 31 (10.8 μm), and 32 (12.1 μm), respectively.

For the KT-15.85 IIP infrared radiometers at the KIT sites and the SI-111 infrared radiometers at the HiWATER sites, the in situ LST measurements were estimated the radiance emitted by the surface and the downwelling radiance by the atmosphere:

$$T_s = B^{-1}\left[\frac{R - (1-\varepsilon) L_{atm}^{\downarrow}}{\varepsilon} \right] \quad (5)$$

where B is the Planck function convolved with the spectral response function of the infrared radiometer, R is the radiance emitted by the surface, which is obtained from the measurements of the infrared radiometer, ε is the surface emissivity for the radiometer spectral channel, and $L_{atm}^{\downarrow}$ is the downwelling radiance convolved with the spectral response function of the infrared radiometer. $L_{atm}^{\downarrow}$ is equivalent to the radiance measured by a radiometer that views the sky at an effective angle of approximately 53° from zenith.

4.2. Temperature-based validation

The temperature-based validation method involves a direct comparison of

ground-based LST measurements and satellite-derived LST products (Coll et al., 2005; Wang et al., 2008; Wang & Liang, 2009; Guillevic et al., 2012, 2014; Göttsche et al., 2013; Ermida et al., 2014; Li et al., 2014; Krishnan et al., 2015). It allows determining the uncertainties in satellite-derived LST products. In this study, the in situ LST measurements estimated from the radiometers were used to evaluate the accuracies of the C6 MODIS LST products (MOD11_L2 and MYD11_L2).

The LST values of the MOD11_L2 and MYD11_L2 products were extracted for the pixel closest to each site in terms of longitude and latitude information. To minimize the effect of cloud contamination on validation results, only the LST values with high-quality data (i.e., QC=0) were used for evaluation. The MODIS LST was matched with the in situ LST using the satellite observation time.

4.3. Robust outlier removal

To obtain robust statistics of LST validation, it is necessary to remove outliers due to cloud contamination. A popular method for outlier detection is the "3σ-edit rule". It assumes that a data sequence is approximately normally distributed and a point further than three standard deviations from the mean is regarded as an outlier (Pearson, 2002). The probability that a point is wrongly removed as an outlier is approximately 0.3%. However, the "3σ-edit rule" usually fails in practice because outliers lead to biased estimates of the mean and standard deviation. A robust method for outlier detection is the "3σ-Hampel identifer" (Davies and Gather, 1993). In this method, the mean is replaced by the median, whereas the standard deviation is estimated as:

$$S = 1.4826 \times median\left\{\left|x_i - x_m\right|\right\} \quad (6)$$

where x_m is the median of the data sequence $\{x_i\}$, S is the standard deviation of the data sequence $\{x_i\}$. The constant 1.4826 is chosen to obtain an unbiased estimate of standard deviation for Gaussian data (Pearson, 2002).

In this study, the data sequence $\{x_i\}$ is the differences between the MODIS LST and the in situ LST. The match-up data points with the LST differences less than

283 x_m-3S or larger than x_m+3S are regarded as outliers. The "3σ-Hampel identifer" only
284 removes a relatively small fraction of outliers (mainly undetected clouds), typically
285 less than 10% (Göttsche et al., 2013).
286
287 5. Results and analyses
288 5.1. Results for the SURFRAD sites
289 Fig. 4 shows the scatterplots between the C6 MODIS LST and the in situ LST
290 during daytime and night-time at the BND, TBL, FPK, GCM, PSU, and SXF sites.
291 The bias, STD, and RMSE of the differences (LST_{MODIS}-LST_{in_situ}) between the C6
292 MODIS LST and the in situ LST are summarized in Fig. 4.
293 The C6 MODIS LST during daytime is lower than the in situ LST over all sites,
294 except for the BND and FPK sites. The smallest absolute bias (approximately 0.2 K)
295 is obtained for the TBL site, whereas the largest absolute bias (approximately 2.5 K)
296 is achieved for the GCM site. The largest STD and RMSE (approximately 4.4 K and
297 4.6 K) are obtained for the BND site, whereas the smallest STD and RMSE
298 (approximately 1.8 K and 2.4 K) are achieved for the PSU site. The largest STD at the
299 BND site indicates that this site is more heterogeneous and exhibits a higher spatial
300 variability of LST. This is consistent with the results reported by Guillevic et al. (2014)
301 and Wang and Liang (2009).
302 The C6 MODIS LST at night is lower than the in situ LST over all sites, except
303 for the PSU site. The bias varies from approximately -1.5 K for the TBL site to
304 approximately 0.5 K for the PSU site. The STD for all sites is less than 1.5 K, and the
305 RMSE is less than 1.9 K. The statistics during night-time are less than those during
306 daytime, especially in terms of STD and RMSE. The daytime STD is greater than 1.9
307 K for all sites, whereas the night-time STD is less than 1.6 K. Larger daytime STD
308 could be caused by the spatial variability of LST, which is usually more significant
309 during daytime than night-time due to the effects of structural shading, evaporative
310 cooling, and surface-air temperature differences. Therefore, the in situ LST
311 measurements during night-time are more representative of the LST at the satellite
312 pixel scale. This is the reason why Wang et al. (2008) only used ground-based LST

measurements during the night to validate the MODIS LST products.

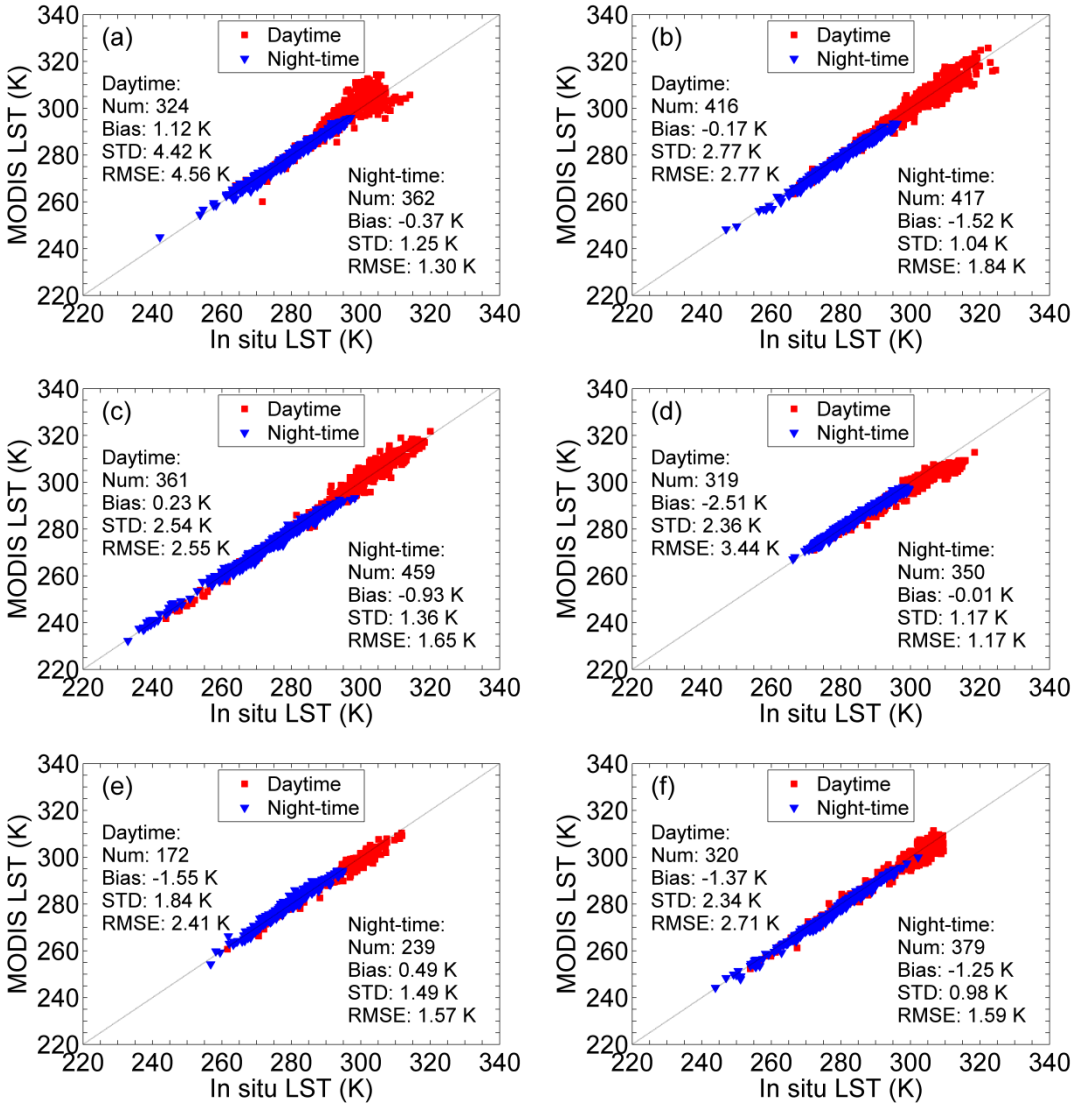

Fig. 4. Scatterplots between the C6 MODIS LST and the in situ LST during daytime and night-time at the six SURFRAD sites, i.e., (a) BND, (b) TBL, (c) FPK, (d) GCM, (e) PSU, and (f) SXF.

To investigate the influences of seasonal variations on LST validation results, we divided all LSTs at each site into four groups in terms of four seasons. Fig. 5 shows the RMSE of the differences (LST_{MODIS}-LST_{in_situ}) between the C6 MODIS LST and the in situ LST during daytime and night-time in four seasons at the six sites. Strong seasonal variations of the RMSE can be found during daytime. The largest RMSE is obtained in summer, whereas the smallest RMSE is achieved in winter at all sites.

Relatively larger RMSE can be found in four seasons at the BND site. The reason is because this site is more heterogeneous and exhibits a higher spatial variability of LST. Larger RMSE in spring at the BND site could be attributed to cloud contamination over snow/ice surfaces (Liu et al., 2015). The seasonal variations are also reported in MODIS and VIIRS LST validation at the SURFRAD sites (Li et al., 2014; Liu et al., 2015). However, there are no significant seasonal variations of the RMSE during night-time. The RMSE during night-time is less than approximately 2 K in four seasons at all sites. The better night-time performance is expected because the thermal heterogeneity is usually higher during daytime and the atmospheric CWV is lower and the land surface behaves almost homogeneously at night.

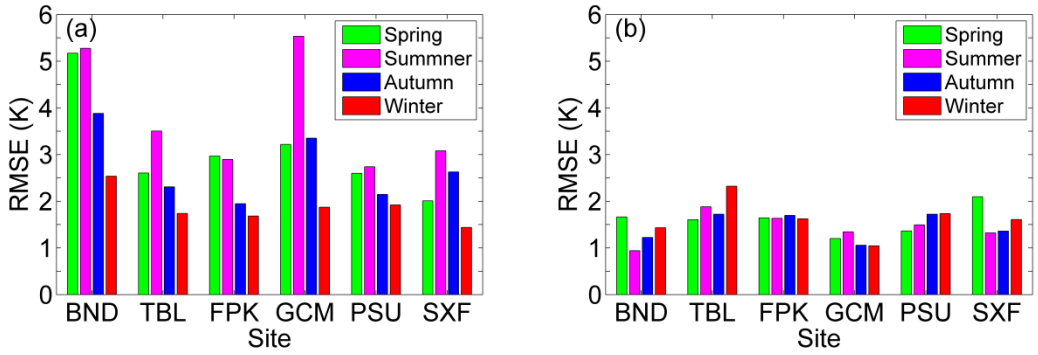

Fig. 5. Bar plots of the RMSE of the differences (LST_{MODIS}-LST_{in_situ}) between the C6 MODIS LST and the in situ LST during (a) daytime and (b) night-time in spring, summer, autumn, and winter at the six SURFRAD sites.

Atmospheric water vapor absorption is one of the most relevant error sources in LST retrieval. To further analyze the effects of atmospheric water vapor on LST validation results, we divided all atmospheric CWV at each site into four groups in terms of four seasons. Fig. 6 displays atmospheric CWV derived from the C6 MODIS atmospheric profile products (MOD07_L2 and MYD07_L2) during daytime and night-time in four seasons at the six sites. Similar pattern of seasonal variations of atmospheric CWV can be found during daytime and night-time. The highest CWV is obtained in summer, whereas the lowest CWV is achieved in winter. However, the atmospheric CWV during night-time is lower than the corresponding value during

daytime in four seasons at all sites. Compared Fig. 5a with Fig. 6a, the seasonal variations of the RMSE of the LST discrepancies during daytime could be attributed to the seasonal variations of the atmospheric CWV. Larger RMSE of the daytime LST discrepancies occur in summer under warm and humid atmospheric conditions. Moreover, smaller RMSE of the night-time LST discrepancies in four seasons could be due to lower LST and atmospheric CWV at night.

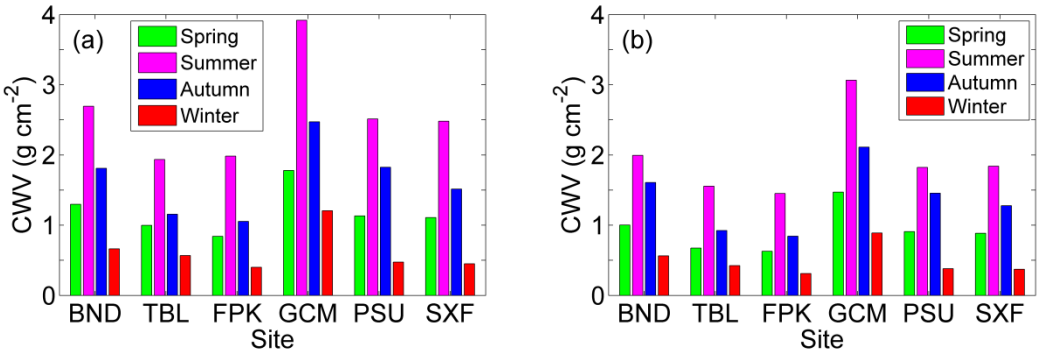

Fig. 6. Bar plots of atmospheric CWV derived from the C6 MODIS atmospheric profile products (MOD07_L2 and MYD07_L2) during (a) daytime and (b) night-time in spring, summer, autumn, and winter at the six SURFRAD sites.

5.2. Results for the KIT sites

Fig. 7 displays the comparison of the C6 MODIS LST and the in situ LST during daytime and night-time at the Evora and Gobabeb sites. The bias, STD, and RMSE of the differences (LST_{MODIS}-LST_{in_situ}) between the C6 MODIS LST and the in situ LST are shown in Fig. 7.

For the results at the Evora site, the C6 MODIS LST is lower than the in situ LST during the day, with a bias of approximately -1.6 K, whereas the situation is reversed at night, with a bias of approximately 0.7 K. The daytime STD and RMSE (approximately 3 K) are approximately twice larger than those (approximately 1.5 K) at night. More dispersion of the LST discrepancies during daytime is due to higher contrast between shaded and sunlit background LST. During night-time, the LST contrast between surface elements, i.e., canopy and background, is very small. Because of their lower dependency on differential heating/cooling (induced by the

existence of shaded and sunlit areas), night-time data are the most reliable for validating satellite-derived LST products (Trigo et al., 2008).

For the results at the Gobabeb site, the C6 MODIS LST is slightly higher than the in situ LST during daytime and night-time, with a bias of approximately 0.3 K. The daytime STD and RMSE (approximately 1.5 K) are approximately twice larger than those (approximately 0.7 K) at night. The results indicate that the C6 MODIS LST is in excellent agreement with the in situ LST at the Gobabeb site, especially at night with accuracy better than 0.8 K.

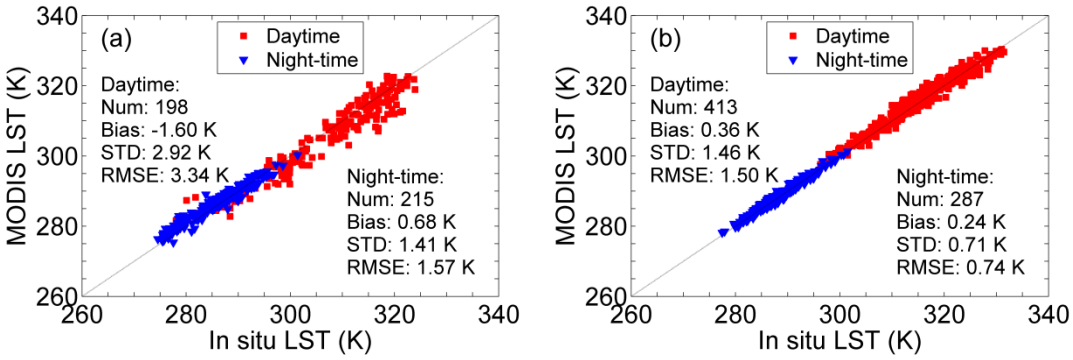

Fig. 7. Scatterplots between the C6 MODIS LST and the in situ LST during daytime and night-time at the two KIT sites, (a) Evora and (b) Gobabeb.

As mentioned in Section 2, three refinements of the GSW LST algorithm were performed in the C6 MODIS LST products over bare soil surfaces. The Gobabeb site is located on large gravel plains (several thousand km^2), which are covered by a highly homogeneous mixture of gravel, sand, and sparse desiccated grass. To investigate whether the C6 MODIS LST products have better performance over bare soil surfaces, we compared the C5 and C6 MODIS LST products at the Gobabeb site. The comparison results are shown in Fig. 8. The accuracies of the C6 MODIS LST products are much better than those of the C5 MODIS LST products. Two reasons can explain the better performance of the C6 MODIS LST products. One reason is that two separate sets of coefficients were used in the C6 GSW algorithm for daytime and night-time LST retrievals over bare soil surfaces. The two sets of GSW coefficients accounts for a wider range of atmospheric and LST conditions over bare soil surfaces.

The other reason could be attributed to the application of the emissivity adjustment model over bare soil surfaces. The C5 MODIS emissivities in bands 31 and 32 are nearly a constant (ε_{31}=0.964 and ε_{32}=0.972) throughout the whole year at the Gobabeb site. Similar results are obtained for the C6 MODIS emissivities in bands 31 and 32 (ε_{31}=0.962 and ε_{32}=0.976). The mean of the emissivities in bands 31 and 32 for C5 and C6 is nearly equal. However, the difference of the emissivities in bands 31 and 32 changes from 0.008 for C5 to 0.014 for C6. Wan (2014) pointed out that the GSW algorithm is more sensitive to the change in the difference of the emissivities in bands 31 and 32 than that in their mean.

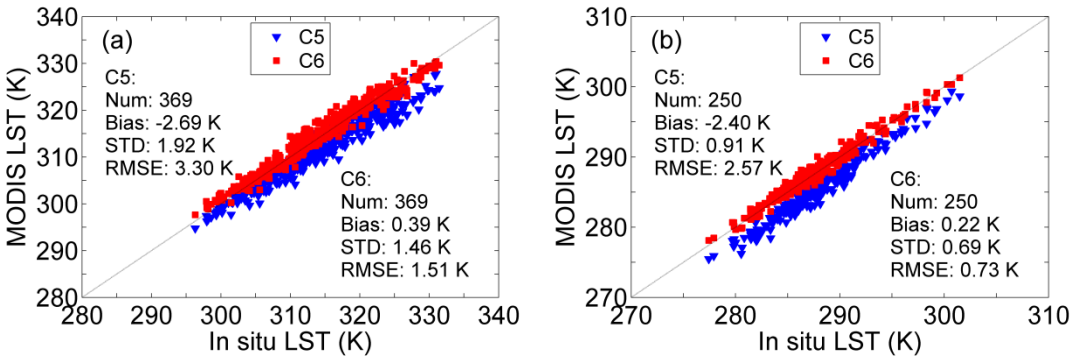

Fig. 8. Scatterplots between the C5 (C6) MODIS LST and the in situ LST during (a) daytime and (b) night-time at the Gobabeb site. Each pair of the corresponding C5 and C6 pixels used for LST validation is the same pixel. The number of pixels is slightly less than that shown in Fig. 7b due to different version of QC data.

5.3. Results for the HiWATER sites

Fig. 9 shows the scatterplots of the C6 MODIS LST versus the in situ LST during daytime and night-time at the GB, SSW, HZZ, and JCHM sites. The bias, STD, and RMSE of the differences (LST_{MODIS}-LST_{in_situ}) between the C6 MODIS LST and the in situ LST are summarized in Fig. 9.

The C6 MODIS LST during the day is lower than the in situ LST at all sites, with the bias varying from approximately -2.5 K for the GB site to approximately -4.7 K for the JCHM site. Larger STD and RMSE during daytime are obtained at the four sites, with STD > 2.2 K and RMSE > 3.3 K. These results indicate that the C6

MODIS LST products underestimate the daytime LST at the four sites due to an overestimation of surface emissivities.

The C6 MODIS LST at night is lower than the in situ LST at all sites except for the HZZ site. The absolute bias varies from approximately 0.2 K for the HZZ site to approximately 2.6 K for the SSW site. Except for the SSW site with a STD of approximately 1.3 K, the STD at the other sites less than 1 K. The results indicate that there are relatively large spatial variations in LST at the SSW site, which is consistent with the results reported by Li et al. (2014). Compared with the daytime results, the night-time results have better accuracies. This is because the atmospheric CWV is lower and the land surface behaves almost homogeneously at night. Therefore, the in situ LST during night-time is more representative of satellite-derived LST than that during daytime.

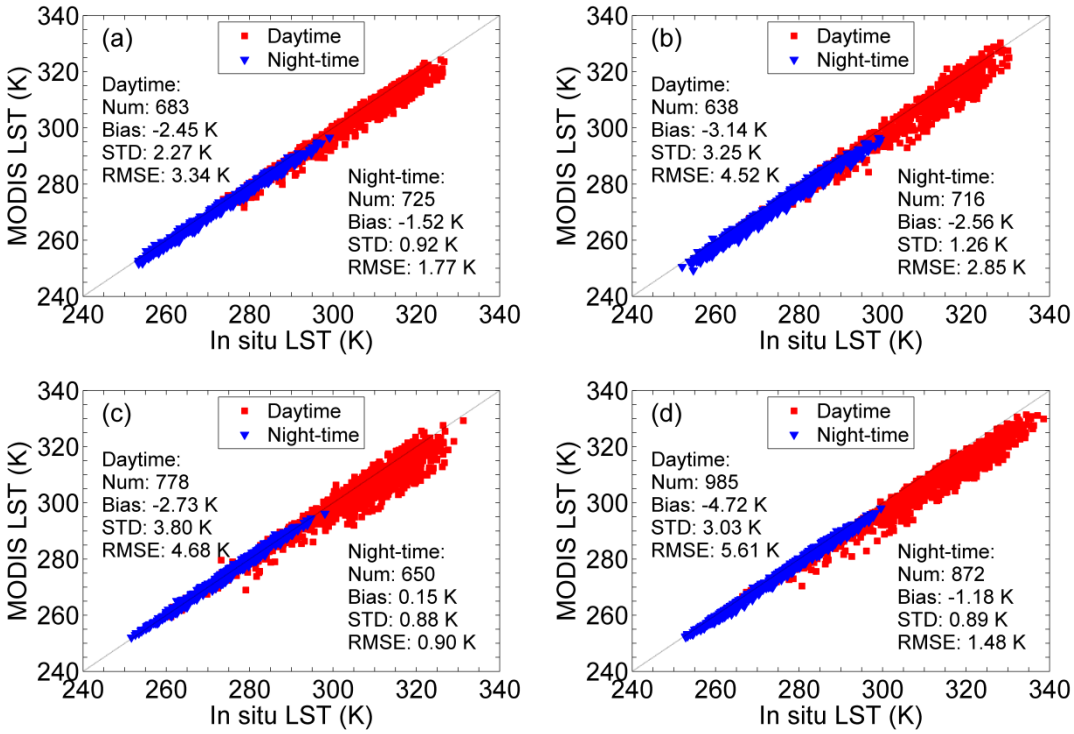

Fig. 9. Scatterplots between the C6 MODIS LST and the in situ LST during daytime and night-time at the four HiWATER sites, i.e., (a) GB, (b) SSW, (c) HZZ, and (d) JCHM.

The four HiWATER sites are located over bare soil surfaces. To evaluate the

448 performance of the C6 MODIS LST products over bare soil surfaces, we compared
449 the C5 and C6 MODIS LST products at the four sites. Fig. 10 displays the bias, STD,
450 and RMSE of the differences (LST_{MODIS}-LST_{in_situ}) between the C5 (C6) MODIS LST
451 and the in situ LST during daytime and night-time at the four sites. There are no
452 improvements in the accuracies of the C6 MODIS LST products when compared with
453 the C5 MODIS LST products. The accuracies of the C6 MODIS LST products are
454 even slightly lower than those of the C5 MODIS LST products in terms of the RMSE.
455 To analyze the reasons for the worse performance of the C6 MODIS LST products,
456 we calculated the mean and STD of the C5 (C6) MODIS emissivities in bands 31 and
457 32 at the four sites. The results are summarized in Table 4. For comparison, the mean
458 and STD of the ASTER emissivity in band 14 given by Li et al. (2014) are also shown
459 in Table 4. Compared with the C5 MODIS emissivities, the emissivity adjustment
460 model leads to the increase in both of the C6 MODIS emissivities in bands 31 and 32
461 at the four sites. The further overestimation of surface emissivities leads to the more
462 underestimation of LST. The C5 MODIS emissivity in band 31 (11.03 μm) is closer to
463 the ASTER emissivity in band 14 (11.3 μm) than the C6 MODIS emissivity is. These
464 results indicate that the improvements in the C6 MODIS LST algorithm do not take
465 effect at the four sites.
466
467 Table 4. Mean and STD of the C5 (C6) MODIS emissivities in bands 31 and 32 at the
468 four HiWATER sites. For comparison, the mean and STD of the ASTER emissivity in
469 band 14 are also shown.

Site	MODIS C5		MODIS C6		ASTER *
	ε_{31} (11.03 μm)	ε_{32} (12.02 μm)	ε_{31} (11.03 μm)	ε_{32} (12.02 μm)	ε_{14} (11.3 μm)
GB	0.971±0.001	0.976±0.001	0.978±0.005	0.982±0.004	0.965±0.002
SSW	0.967±0.002	0.973±0.002	0.973±0.004	0.978±0.003	0.958±0.001
HZZ	0.975±0.003	0.979±0.003	0.984±0.001	0.988±0.001	0.973±0.003
JCHM	0.969±0.002	0.974±0.001	0.984±0.001	0.988±0.001	0.973±0.002

470 * Source: Li et al. (2014).

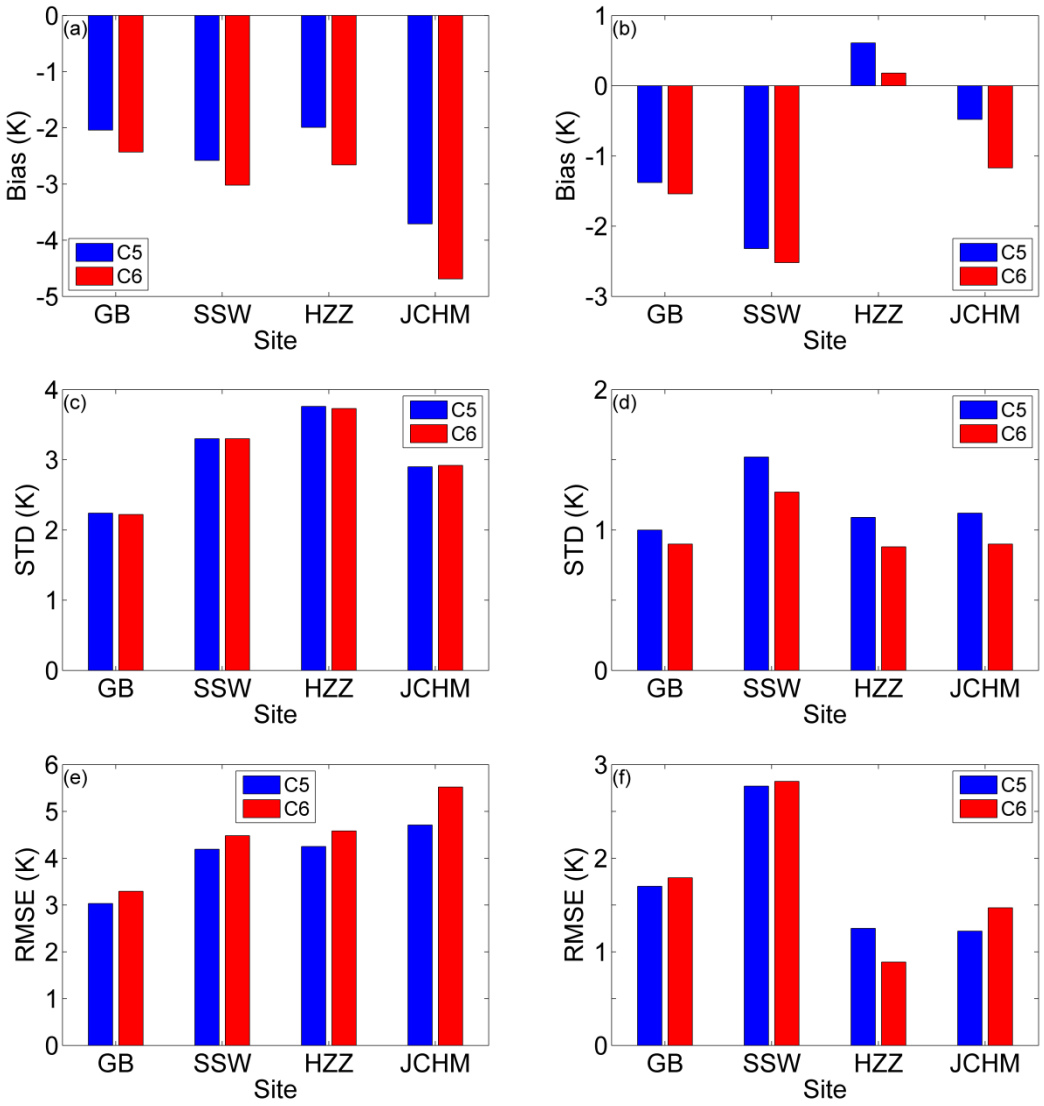

Fig. 10. Bar plots of the bias, STD, and RMSE of the differences (LST_{MODIS}-LST_{in_situ}) between the C5 (C6) MODIS LST and the in situ LST during (a) daytime and (b) night-time at the four HiWATER sites.

6. Discussion

6.1. Issues of the MODIS C6 LST products

Three refinements were implemented in the C6 MODIS LST products over bare soil surfaces, but some issues are still found in the C6 MODIS LST products. In addition to the effects of sensor calibration, geolocation errors, and cloud masking, atmospheric water vapor absorption and surface emissivity uncertainty are two most relevant error sources in LST retrieval.

Over the past few decades, great efforts have been made to improve the

accuracies of satellite-derived LST products from thermal infrared data, e.g., NOAA, MODIS, VIIRS, and ASTER. A comprehensive review of TIR LST retrieval algorithms were presented by Li et al. (2013a). Accurate characterization of atmospheric effects in these LST retrieval algorithms under warm and humid conditions is still a challenging task. As shown in Fig. 5a, the C6 MODIS LST products have larger RMSE of the LST discrepancies in summer when both of atmospheric CWV and LST are high. In previous studies, inaccurate characterizations of atmospheric effects under warm and humid conditions were also observed in the VIIRS (Guillevic et al., 2014) and ASTER (Gillespie et al., 2011) LST products.

The MODIS GSW LST algorithm used the classification-based emissivity method to correct the effects of surface emissivity. The key point of this method is to properly classify the land surface and then to assign the emissivity from classification-based look-up tables (Snyder et al., 1998; Li et al., 2013b). The classification-based emissivity method could result in surface emissivity uncertainty in two aspects. One aspect is that the accuracy of emissivity estimation depends on the accuracy of the land cover type product. Misclassifications in the land cover type product would lead to emissivity errors. The other aspect is that emissivities used in the MODIS GSW LST algorithm were derived from fixed values depending on a limited number of land cover types and do not fully encompass the natural variation in emissivity, especially over bare soil surfaces. The incorporation of a dynamic emissivity product generated by the temperature and emissivity separation (TES) algorithm (Hulley and Hook, 2011) into the GSW LST algorithm would be a way to further improve the accuracies of the MODIS LST products, especially over bare soil surfaces.

The emissivity adjustment model was used in the C6 MODIS GSW LST algorithm to adjust emissivity over bare soil surfaces (Wan, 2014). This model is useful to reduce the C6 MODIS LST errors. As shown in Fig. 8, the accuracies of the C6 MODIS LST products (RMSE of approximately 1.5 K during daytime and approximately 0.7 K during night-time) are much better than those of the C5 MODIS LST products (RMSE of approximately 3.3 K during daytime and approximately 2.6

K during night-time) at the Gobabeb site. However, the emissivity adjustment model could also lead to further overestimation or underestimation of emissivities at some sites. As shown in Fig. 10 and Table 4, the further overestimation of emissivities leads to the more underestimation of the C6 MODIS LST products at the four HiWATER sites, when compared with the C5 MODIS LST products. Furthermore, Wan (2014) reported that the emissivity adjustment model leads to the further underestimation of emissivities at the Farafra site. The mean error of LST at the Farafra site increases from 1.01 K for the C5 MODIS LST products to 1.87 K for the C6 MODIS LST products.

6.2. Challenges of temperature-based validation

As pointed out by Yu et al. (2012), there are many challenges in the temperature-based validation of satellite-derived LST products. Because of large spatial variations in LST, in situ LST measurements are difficult to represent LST measurements at the satellite pixel scale, especially during daytime. As shown in Section 5, large uncertainties in LST can be found during daytime, with RMSE value up to 5.6 K at the JCHM site. Because atmospheric water vapor is less and the land surface behaves more homogeneously at night, in situ LST measurements during night-time are more representative of LST at the satellite pixel scale. Therefore, Wang et al. (2008) only used ground-based LST measurements during the night to validate the MODIS LST products.

To obtain high quality data from ground-based LST measurements to validate satellite-derived LST products, previous studies conducted field campaigns only over large homogeneous sites, such as lake, snow, grassland, silt playa, and cropland fields (Wan et al., 2002, 2004; Coll et al., 2005, 2009). Fig. 11 shows the scatterplots between the C6 MODIS LST and the in situ LST at the sites of Wan et al. (2002, 2004) and Coll et al. (2016). The RMSE of the LST discrepancies is less than 1 K. The results indicate that the temperate-based validation can provide suitable validation results for well-defined and dedicated sites. Therefore, quantitative assessment of satellite-derived LST products requires dedicated and high quality in situ LST

measurements over sites that are homogeneous at the satellite pixel scale. Moreover, it is necessary to use multiple TIR radiometers with high accuracy at multiple points within a satellite pixel to well characterize the validate site.

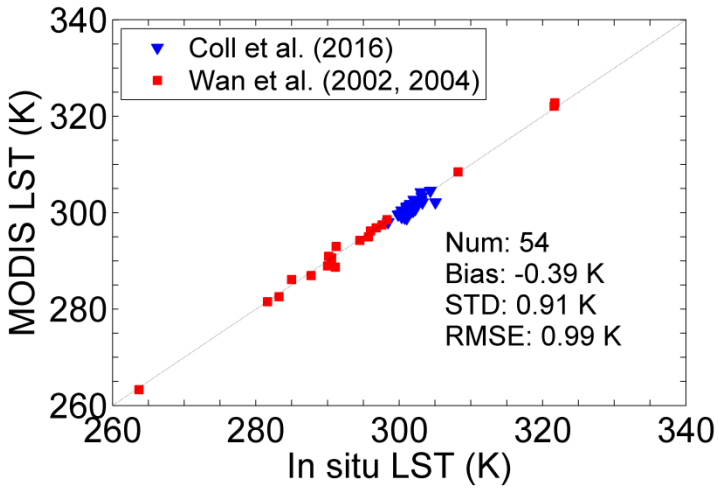

Fig. 11. Scatterplots between the C6 MODIS LST and the in situ LST at the sites of Wan et al. (2002, 2004) and Coll et al. (2016).

TIR field radiometers always collect ground-based measurements at nadir, whereas satellite sensors with wide field-of-view, e.g., MODIS, AVHRR, and VIIRS, collect most observations off-nadir. Such observation difference could be a possible reason resulting in the discrepancies between in situ LST and satellite-derived LST. On the one hand, larger VZA results in longer atmospheric optical length. Significant decrease of atmospheric transmittance with increase of atmospheric water vapor introduces significant errors in the GSW algorithm when LST is high. On the other hand, larger VZA leads to larger discrepancies of observed targets and their areas between TIR field radiometers and satellite sensors, especially over spatially heterogeneous validation sites. To investigate the effects of the observation difference, we compared the C6 MODIS LST with VZA less than 30° with the situ LST during daytime and night-time at the four HiWATER sites. The results are shown in Fig. 12. Compared with the results in Figs. 9 and 12, the bias, STD, and RMSE with VZA less than 30° are better than those with all VZA, especially during daytime.

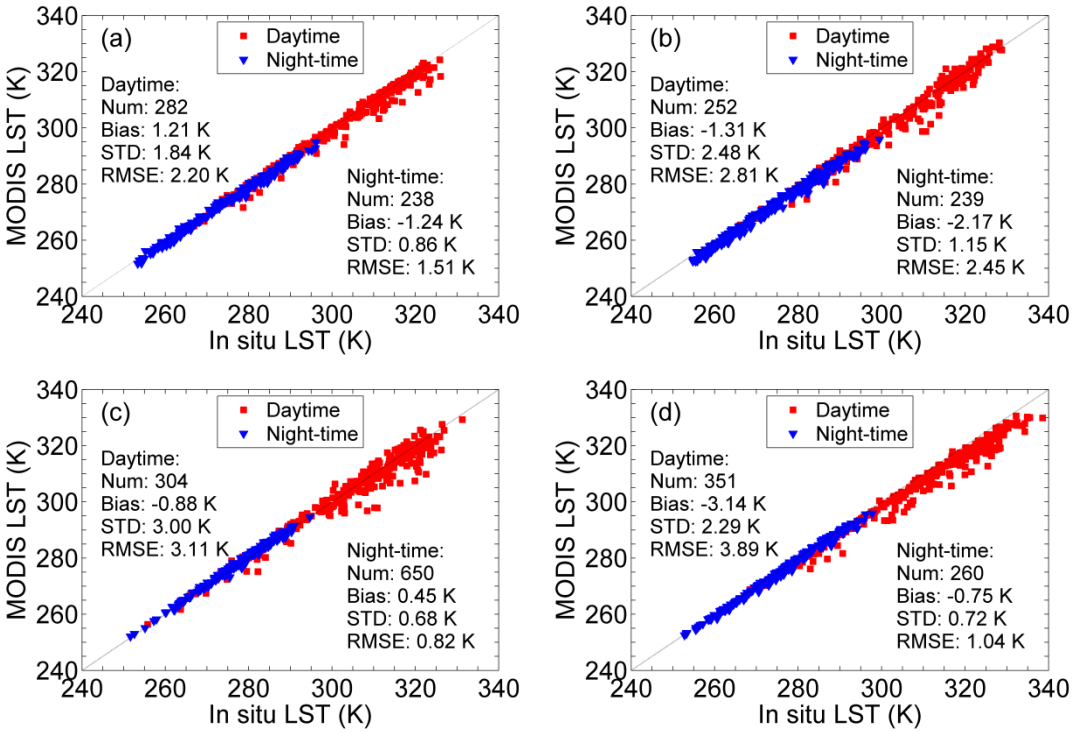

Fig. 12. Scatterplots between the C6 MODIS LST with VZA less than 30° and the in situ LST during daytime and night-time at the four HiWATER sites, i.e., (a) GB, (b) SSW, (c) HZZ, and (d) JCHM.

7. Conclusions

We validated the C6 MODIS LST products using in situ measurements collected from sites under different atmospheric and surface conditions, including six SURFRAD sites in the United States, two KIT sites in Portugal and Namibia, and four HiWATER sites in China.

The average bias and RMSE during daytime at the six SURFRAD sites are -0.71 K and 3.07 K, respectively, whereas those at night are -0.6 K and 1.52 K, respectively. Significant seasonal variations of the RMSE can be found during daytime. The largest RMSE is obtained in summer, whereas the smallest RMSE is achieved in winter at the six SURFRAD sites. Inaccurate characterizations of atmospheric effects under warm and humid conditions are observed in summer when both of atmospheric CWV and LST are high. There are no significant seasonal variations of the RMSE at night. The night-time RMSE is less than approximately 2 K in four seasons at the six SURFRAD sites.

588 Compared with the C5 MODIS LST products, the C6 MODIS LST products are
589 in excellent agreement with the in situ LST measurements at the Gobabeb site, with
590 biases of 0.36 K during the day and 0.24 K at night, and RMSEs of 1.5 K during
591 daytime and 0.74 K during night-time. The results show that the emissivity
592 adjustment model incorporated into the C6 MODIS GSW LST algorithm is useful to
593 reduce the C6 MODIS LST errors over bare soil surfaces. However, the emissivity
594 adjustment model leads to further overestimation of emissivities at the four
595 HiWATER sites. There are no improvements in the accuracies of the C6 MODIS LST
596 products when compared with the C5 MODIS LST products. The RMSEs of the C6
597 MODIS LST products are even slightly larger than those of the C5 MODIS LST
598 products. The results indicated that the classification-based emissivity method cannot
599 well characterize the spectral variation in emissivity over bare soil surfaces. The
600 incorporation of a dynamic LSE product generated by the TES algorithm into the
601 GSW LST algorithm would be a way to further improve the accuracies of the MODIS
602 LST products.

603 The accuracies of the C6 MODIS LST products at night are better than those
604 during daytime. The daytime RMSE varies from approximately 1.5 K at the Gobabeb
605 site to approximately 5.6 K at the JCHM site, whereas the night-time RMSE is less
606 than 2 K at all sites except for the SSW site. The results indicate that night-time data
607 are the most reliable for the validation of satellite-derived LST products due to lower
608 atmospheric water vapor and more homogeneous of the land surface. To
609 comprehensively evaluate the accuracies of satellite-derived LST products, the
610 radiance-based validation method can be used to validate daytime LST products over
611 a more diverse set of conditions on a global scale.

612

613 References

614 Anderson, M. C., Norman, J. M., Kustas, W. P., Houborg, R., Starks, P. J., & Agam, N.
615 (2008). A thermal-based remote sensing technique for routine mapping of
616 land-surface carbon, water and energy fluxes from field to regional scales.
617 Remote Sensing of Environment, 112, 4227-4241.
618 Augustine, J. A., DeLuisi, J. J., & Long, C. N. (2000). SURFRAD—A national

surface radiation budget network for atmospheric research. Bulletin of the American Meteorological Society, 81, 2341-2357.
Becker, F., & Li, Z.-L. (1990). Towards a local split window method over land surfaces. International Journal of Remote Sensing, 11, 369-393.
Coll, C., Caselles, V., Galve, J. M., Valor, E., Niclòs, R., Sánchez, J. M., & Rivas, R. (2005). Ground measurements for the validation of land surface temperatures derived from AATSR and MODIS data. Remote Sensing of Environment, 97, 288-300.
Coll, C., Wan, Z., & Galve, J. M. (2009a). Temperature-based and radiance-based validations of the V5 MODIS land surface temperature product. Journal of Geophysical Research, 114, D20102.
Coll, C., García-Santos, V., Niclòs, R., & Caselles, V. (2016). Test of the MODIS land surface temperature and emissivity separation algorithm with ground measurements over a rice paddy. IEEE Transactions on Geoscience and Remote Sensing, 54, 3061-3069.
Davies, L., & Gather, U. (1993). The identification of multiple outliers. Journal of the American Statistical Association, 88, 782-792.
Duan, S.-B., Li, Z.-L., Tang, B.-H., Wu, H., & Tang, R. (2014). Generation of a time-consistent land surface temperature product from MODIS data. Remote Sensing of Environment, 140, 339-349.
Ermida, S. L., Trigo, I. F., DaCamara, C. C., Göttsche, F.-M., Olesen, F.-S., & Hulley, G. (2014). Validation of remotely sensed surface temperature over an oak woodland landscape—The problem of viewing and illumination geometries. Remote Sensing of Environment, 148, 16-27.
Gillespie, A. R., Abbott, E. A., Gilson, L., Hulley, G., Jiménez-Muñoz, J.-C., & Sobrino, J. A. (2011). Residual errors in ASTER temperature and emissivity standard products AST08 and AST05. Remote Sensing of Environment, 115, 3681-3694.
Göttsche, F.-M., Olesen, F.-S., & Bork-Unkelbach, A. (2013). Validation of land surface temperature derived from MSG/SEVIRI with in-situ measurements at Gobabeb, Namibia. International Journal of Remote Sensing, 34, 3069-3083.
Göttsche, F.-M., & Hulley, G. C. (2012). Validation of six satellite-retrieved land surface emissivity products over two land cover types in a hyper-arid region. Remote Sensing of Environment, 124, 149-158.
Göttsche, F.-M. , Olesen, F.-S., Trigo, I. F., Bork-Unkelbach, A., & Martin, M. A. (2016). Long term validation of land surface temperature retrieved from MSG/SEVIRI with continuous in-situ measurements in Africa. Remote Sensing, 8, 410.
Guillevic, P. C., Privette, J. L., Coudert, B., Palecki, M. A., Demarty, J., Ottle, C., & Augustine, J. A. (2012). Land Surface Temperature product validation using NOAA's surface climate observation networks---Scaling methodology for the Visible Infrared Imager Radiometer Suite (VIIRS). Remote Sensing of Environment, 124, 282-298.
Guillevic, P. C., Biard, J. C., Hulley, G. C., Privette, J. L., Hook, S. J., Olioso, A.,

Göttsche, F.-M., Radocinski, R., Román, M. O., Yu, Y., & Csiszar, I. (2014). Validation of land surface temperature products derived from the Visible Infrared Imaging Radiometers Suite (VIIRS) using ground-based and heritage satellite measurements. Remote Sensing of Environment, 154, 19-37.

Hulley, G. C., & Hook, S. J. (2011). Generating consistent land surface temperature and emissivity products between ASTER and MODIS data for earth science research. IEEE Transactions on Geoscience and Remote Sensing, 49, 1304-1315.

Kabsch, E., Olesen, F.-S., & Prata, F. (2008). Initial results of the land surface temperature (LST) validation with the Evora, Portugal ground-truth station measurements. International Journal of Remote Sensing, 29, 5329-5345.

Krishnan, P., Kochendorfer, J., Dumas, E. J., Guillevic, P. C., Baker, C. B., Meyers, T. P., & Martos, B. (2015). Comparison of in-situ, aircraft, and satellite land surface temperature measurements over a NOAA Climate Reference Network site. Remote Sensing of Environment, 165, 249-264.

Lambin, E. F., & Ehrlich, D. (1997). Land-cover changes in sub-Saharan Africa (1982–1991): Application of a change index based on remotely-sensed surface temperature and vegetation indices at a continental scale. Remote Sensing of Environment, 61, 181-200.

Leng, P., Song, X. N., Li, Z.-L., Ma, J. W., Zhou, F. C. & Li, S. (2014). Bare surface soil moisture retrieval from the synergistic use of the optical and thermal infrared data. International Journal of Remote Sensing, 35: 988-1003.

Li, H., Sun, D., Yu, Y., Wang, H., Liu, Y., Liu, Q., Du, Y., Wang, H., & Cao, B. (2014). Evaluation of the VIIRS and MODIS LST products in an arid area of Northwest China. Remote Sensing of Environment, 142, 111-121.

Li, S., Yu, Y., Sun, D., Tarpley, D., Zhan, X., & Chiu, L. (2014). Evaluation of 10 year AQUA/MODIS land surface temperature with SURFRAD observations. International Journal of Remote Sensing, 35, 830-856.

Li, X., Cheng, G., Liu, S., Xiao, Q., Ma, M., Jin, R., et al. (2013). Heihe watershed allied telemetry experimental research (HiWATER): Scientific objectives and experimental design. Bulletin of the American Meteorological Society, 94, 1145 – 1160.

Li, Z.-L., Tang, B.-H., Wu, H., Ren, H., Yan, G., Wan, Z., Trigo, I. F., & Sobrino, J. A. (2013). Satellite-derived land surface temperature: Current status and perspectives. Remote Sensing of Environment, 131, 14-37.

Li, Z.-L., Wu, H., Wang, N., Qiu, S., Sobrino, J. A., Wan, Z., Tang, B.-H., & Yan, G. (2013). Land surface emissivity retrieval from satellite data. International Journal of Remote Sensing, 34, 3084-3127.

Liu, Y., Yu, Y., Yu, P., Göttsche, F.-M. & Trigo, I. F. (2015). Quality assessment of S-NPP VIIRS land surface temperature product. Remote Sensing, 7, 12215-12241.

Lu, J., Tang, R., Tang, H., & Li, Z.-L. (2013). Derivation of daily evaporative fraction Based on temporal variations in surface temperature, air temperature, and net radiation. Remote Sensing, 5, 5369-5396.

Pearson, R. K. (2002). Outliers in process modeling and identification. IEEE

Transactions on Control Systems Technology, 10, 55-63.
Sandholt, I., Rasmussen, K., & Andersen, J. (2002). A simple interpretation of the surface temperature/vegetation index space for assessment of surface moisture status. Remote Sensing of Environment, 79, 213-224.
Snyder, W. C., Wan, Z., Zhang, Y., & Feng, Y.-Z. (1998). Classification-based emissivity for land surface temperature measurement from space. International Journal of Remote Sensing, 19, 2753-2774.
Trigo, I. F., Monteiro, I. T., Olesen, F., & Kabsch, E. (2008a). An assessment of remotely sensed land surface temperature. Journal of Geophysical Research, 113, D17108. doi:10.1029/2008JD010035.
Wan, Z., & Dozier, J. (1996). A generalized split-window algorithm for retrieving land-surface temperature from space. IEEE Transactions on Geoscience and Remote Sensing, 34, 892-905.
Wan, Z., & Li, Z.-L. (1997). A physics-based algorithm for retrieving land-surface emissivity and temperature from EOS/MODIS data. IEEE Transactions on Geoscience and Remote Sensing, 35, 980-996.
Wan, Z., Zhang, Y., Zhang, Q., & Li, Z.-L. (2002). Validation of the land-surface temperature products retrieved from Terra Moderate Resolution Imaging Spectroradiometer data. Remote Sensing of Environment, 83, 163-180.
Wan, Z., Zhang, Y., Zhang, Q., & Li, Z.-L. (2004). Quality assessment and validation of the MODIS global land surface temperature. International Journal of Remote Sensing, 25, 261-274.
Wan, Z., Wang, P., & Li, X. (2004). Using MODIS Land Surface Temperature and Normalized Difference Vegetation Index products for monitoring drought in the southem Great Plains,USA. International Journal of Remote Sensing, 25, 61-72.
Wan, Z. (2008). New refinements and validation of the MODIS land-surface temperature/emissivity products. Remote Sensing of Environment, 112, 59-74.
Wan, Z., & Li, Z.-L. (2008). Radiance-based validation of the V5 MODIS land-surface temperature product. International Journal of Remote Sensing, 29, 5373-5395.
Wan, Z. (2014). New refinements and validation of the collection-6 MODIS land-surface temperature/emissivity product. Remote Sensing of Environment, 140, 36-45.
Wang, K., Wan, Z., Wang, P., Sparrow, M., Liu, J., Zhou, X., & Haginoya, S. (2005). Estimation of surface long wave radiation and broadband emissivity using Moderate Resolution Imaging Spectroradiometer (MODIS) land surface temperature/emissivity products. Journal of Geophysical Research, 110, D11109.
Wang, K., & Liang, S. (2009). Evaluation of ASTER and MODIS land surface temperature and emissivity products using long-term surface longwave radiation observations at SURFRAD sites. Remote Sensing of Environment, 113, 1556-1565.
Wang, W., Liang, S., & Meyers, T. (2008). Validating MODIS land surface temperature products using long-term nighttime ground measurements. Remote Sensing of Environment, 112, 623-635.

751 Weng, Q. (2009). Thermal infrared remote sensing for urban climate and
752 environmental studies: methods, applications, and trends. ISPRS Journal of
753 Photogrammetry and Remote Sensing, 64, 335-344.
754 Xu, H., Yu, Y., Tarpley, D., Göttsche, F.-M., & Olesen, F.-S. (2014). Evaluation of
755 GOES-R land surface temperature algorithm using SEVIRI satellite retrievals
756 with in situ measurements. IEEE Transactions on Geoscience and Remote
757 Sensing, 52, 3812-3822.
758 Yu, Y., Tarpley, D., Privette, J. L., Flynn, L. E., Xu, H., Chen, M., Vinnikov, K. Y.,
759 Sun, D., & Tian, Y. (2012). Validation of GOES-R satellite land surface
760 temperature algorithm using SURFRAD ground measurements and statistical
761 estimations of error properties. IEEE Transactions on Geoscience and Remote
762 Sensing, 50, 704-713.
763